



Causes and Evolution of Winter Polynyas over North of Greenland

Younjoo J. Lee¹, Wieslaw Maslowski¹, John J. Cassano^{2,3}, Jaclyn Clement Kinney¹, Anthony P. Craig⁴, Samy Kamal⁵, Robert Osinski⁶, Mark W. Seefeldt^{2,3}, Julienne Stroeve^{2,7}, Hailong Wang⁸

¹Naval Postgraduate School, Monterey, California, USA

5 ²National Snow and Ice Data Center, Boulder, Cooperative Institute for Research in Environmental Sciences, University of Colorado, Boulder, Colorado, USA

³Department of Atmospheric and Oceanic Sciences, University of Colorado, Boulder, Colorado, USA

⁴Independent Researcher

⁵RedLine Performance Solutions, College Park, Maryland, USA

10 ⁶Institute of Oceanology of the Polish Academy of Sciences, Sopot, Poland

⁷University of Manitoba, Winnipeg, Manitoba, Canada

⁸Pacific Northwest National Laboratory, Richland, Washington, USA

Correspondence to: Younjoo J. Lee (ylee1@nps.edu)

15 **Abstract.** During the 42-year period (1979-2020) of satellite measurements, only three winter polynyas have ever been observed north of Greenland and they all occurred in the last decade, i.e. February of 2011, 2017 and 2018. The 2018 polynya was unparalleled by its magnitude and duration compared to the two previous events. Combined with the limited weather station and remotely-sensed sea ice data, a fully-coupled Regional Arctic System Model (RASM) hindcast simulation was utilized to examine the
20 causality and evolution of these recent extreme events. We found that neither the accompanying anomalous warm surface air intrusion nor the ocean below had an impact on the development of these winter open water episodes in the study region (i.e., no significant ice melting). Instead, the extreme atmospheric wind forcing resulted in greater sea ice deformation and transport offshore, accounting for the majority of sea ice loss. Our analysis suggests that strong southerly winds (i.e., northward wind with
25 speeds of greater than 10 m/s) blowing persistently for at least 2 days or more, were required over the study region to mechanically redistribute some of the thickest sea ice out of the region and thus to create open water areas (a latent heat polynya). In order to assess the role of internal variability versus external forcing of such events, we additionally simulated and examined results from two RASM ensembles forced with output from the Community Earth System Model (CESM) Decadal Prediction Large
30 Ensemble (DPLE) simulations. Out of 100 winters in each of the two ensembles, initialized 30 years apart, one in December 1985 and another in December 2015, respectively, 17 and 14 winter polynyas were produced over north of Greenland. The frequency of polynya occurrence and no apparent sensitivity to the initial sea ice thickness in the study area point to internal variability of atmospheric forcing as a dominant cause of winter polynyas north of Greenland. We assert that dynamical
35 downscaling using a high-resolution regional climate model offers a robust tool for process-level examination in space and time, synthesis with limited observations and probabilistic forecast of Arctic events, such as the ones being investigated here and elsewhere.



1. Introduction

40 The Arctic has experienced amplified warming, both through the enhancement of global temperature
rise, as well as through the reductions in sea ice and snow cover that impact the regional energy budget
(Serreze and Francis, 2006). This is commonly referred to as Arctic amplification (AA). On a seasonal
basis, Arctic winter warming (AWW) exceeds summer warming by about a factor of four (Bintanja and
van der Linden, 2013). In addition to sea ice variations, changes in the atmospheric circulation have
45 been linked to an increase in frequency and duration of winter warming events in the Arctic (Graham et
al., 2017). The trends in AWW and winter sea ice extent (SIE) have continued over the satellite record,
with the March SIE decline rate of $\sim 2.6\%$ per decade for the period of 1979-2020, including the four
lowest winter maxima of SIE in 2015-2018 and the lowest ten during 2005-2019. While SIE reductions
in winter are less than ones in summer (Stroeve and Notz, 2018), there is clear supporting evidence that
50 the winter ice pack has thinned and the amount of multi-year sea ice has declined (Kwok et al., 2009;
Meier et al., 2014; Kwok, 2018). It is expected that the resulting younger and thinner ice is more
susceptible to atmospheric wind forcing (Spreen et al., 2011; Itkin et al., 2017), yielding increased sea
ice drift speed, enhanced fracturing and more lead openings (Rampal et al., 2009). Hence, along with
the current trend in the Arctic sea ice toward younger and thinner ice, it can be hypothesized that
55 polynyas may become more prevalent in recent years. Since about half of the total atmosphere-ocean
heat exchange over the Arctic Ocean may occur through leads and polynyas in winter (Maykut, 1982),
the occurrence and formation of polynyas could play a crucial role in the alteration of regional climate
(Morales Maqueda et al., 2004).

In late February 2018, satellite imagery revealed an unusual open water polynya over north of
60 Greenland between the Lincoln and Wandel seas (Fig. 1a). This event received considerable attention
not only because it was claimed to be a one-of-a-kind extreme event involving some of the thickest
Arctic sea ice but also because its emergence coincided with anomalous, above freezing, warming of
surface air temperature over the region (Moore et al., 2018). The presumed contribution of this warm
surface air to the polynya opening is of interest and so are its causality, evolution and past occurrences.
65 Yet, detailed *in situ* observations of polynyas are limited due to their intermittency and restricted access
in winter. Hence, in addition to satellite measurements and weather data, fully coupled climate models
become critical tools in studying such events (e.g., Ludwig et al., 2019). However, for the majority of
global climate models (GCMs), many coastal polynyas are at sub-grid scales; thus, the GCM utility for
comprehensive polynya studies are impeded (Weijer et al., 2017). In addition, GCMs are not intended to
70 represent specific climate events in space and time and they are not suitable for process-level
investigation of such events and quantification of their impact at both local and larger scales.

On the other hand, regional climate models (RCMs) used for dynamical downscaling are expected to
show improvement in reproducing extreme weather events, given that their atmospheric boundary
75 conditions for simulations of the past to present are derived from global atmospheric reanalysis such as
Climate Forecast System (CFS) version 2 (CFSv2; Saha et al., 2011). Therefore, high-resolution RCMs,
such as the Regional Arctic System Model (RASM; e.g. Maslowski et al. 2012), offer unique
capabilities for examining the spatio-temporal development and impact of observed specific events like



80 a polynya (Fig. 1b), in the context of a fully-coupled climate system model (atmosphere-sea ice-ocean-land), while CFSv2 is shown to be less skillful in simulating such an event (Fig. 1c). In addition, RCMs afford ensemble sizes prohibitive to their global fine-resolution counterparts, which is often a requirement to distinguish the forced response from internal model variability (e.g., Peings et al. 2021).

85 The 2018 winter polynya over north of Greenland has been investigated by Moore et al. (2018) using an ice-ocean model forced by surface atmospheric reanalysis. They have established the dominant role of surface winds in generating this polynya. Here, by taking advantage of the fully-coupled and high-resolution RASM hindcast simulation, combined with weather station and satellite sea ice data, we evaluate the capability of RCM in reproducing the observed natural phenomena (Fig. 2) and investigate the coupled mechanisms involved in the development of northern Greenland coastal polynyas within
90 some of the thickest Arctic ice-pack cover. In particular, this study focuses on analysis of historical winter polynya events for the full period of satellite data availability (1979-2020) to diagnose the relative roles of thermodynamic and dynamic processes and to assess required forcing changes over the last four decades. Furthermore, by dynamic downscaling of the Community Earth System Model (CESM)-Decadal Prediction Large Ensemble (DPLE), two sets of 30 years apart RASM ensemble
95 (termed RASM-DPLE) simulations are performed to examine the relative roles of internal variability and external forcing influencing the development of winter polynyas under two different sea ice regime scenarios: i.e. a thicker ice in the 1980s versus a thinner ice in the 2010s. We provide details of the satellite and weather station data used for this study in section 2 and the model setup for the hindcast and DPLE simulations are described in section 3. Next, section 4 presents a synthesis of observed and
100 modeled past winter polynya results and examines the statistics of polynya occurrence and the required conditions for their generation in the RASM-DPLE simulations. This is followed by the discussion in section 5 and the study is summarized in section 6.

2 Data

2.1. Surface air temperature and wind

105 Hourly surface air temperature (3-hourly prior to 2015) data were obtained from the seven weather stations (World Meteorological Organization station identifier: 04221, 04254, 04285, 04351, 04330, 04312 and 04301) around Greenland (data available at <https://rp5.ru>) and then averaged daily for January-March of 2011, 2017, and 2018. Since wind data were incomplete at the closest weather station from the center of polynya in 2018 (i.e., Station 04301, Cape Morris Jessup at 83° 39' N and 33° 22' W),
110 we used 3-hourly surface wind data from the adjacent Station 04312 (Station Nord at 81°43' N and 17°47' W), which were originally binned for 16 wind directions. Also, ERA-Interim atmospheric reanalysis of 6-hourly 10 m wind fields (Dee et al., 2011; <https://www.ecmwf.int/en/forecasts/datasets/reanalysis-datasets/era-interim>) was used for comparison with the RASM hindcast simulation over the study region.

2.2. Sea ice concentration and thickness



Daily sea ice concentration (SIC) data were obtained via the National Snow and Ice Data Center (NSIDC): <https://nsidc.org/data/nsidc-0051> for 1979–2019 and <https://nsidc.org/data/nsidc-0081> for 2020. Satellite-derived SIC used for this study is based on passive microwave measurements using the
120 NASA team (NT) algorithm (Cavalieri et al., 1984); all the data are on a polar stereographic 25 km×25 km grid. The mean daily SIC was used to detect the occurrence of a polynya in the satellite measurement when it dropped below 90% over the study region. RASM sea ice thickness (SIT) was also compared with the CryoSat-2/the Soil Moisture Ocean Salinity (SMOS) satellite merged data that are only available in winter months from 2011 (<https://www.meereisportal.de>; Grosfeld et al., 2016) as
125 well as CFSv2 reanalysis (<https://doi.org/10.5065/D61C1TXF>). Due to the lack of persistent SIT observations over the Arctic, the Pan-Arctic Ice Ocean Modeling and Assimilation System (PIOMAS) is often considered as an “observational” proxy (Zhang and Rothrock 2003; Schweiger et al. 2011; Stroeve et al. 2014). The PIOMAS (version 2.1) sea ice data were retrieved from the Polar Science Center at the University of Washington (<http://psc.apl.uw.edu/research/projects/arctic-sea-ice-volume-anomaly/data/>).
130

3 Method

3.1 Regional Arctic System Model

RASM is a limited-area, fully-coupled climate model consisting of the Weather Research and
135 Forecasting (WRF version 3.7.1) for atmosphere, the Los Alamos National Laboratory Sea Ice Model (CICE version 5.1.2) for sea ice and Parallel Ocean Program (POP version 2.1) for ocean, the Variable Infiltration Capacity (VIC version 4.0.6) land hydrology and routing scheme (RVIC version 1.0.0) for land (see Maslowski et al. 2012; Roberts et al. 2015; DuVivier et al. 2015; Hamman et al. 2016; Hamman et al. 2017; Cassano et al. 2017). All the components are coupled using the Craig et al. (2012)
140 version of CESM flux coupler. RASM is configured over a pan-Arctic domain, including the entire Northern Hemisphere marine cryosphere and all terrestrial drainage basins that drain to the Arctic Ocean. The ocean and sea ice components share a 1/12-degree (~9 km) rotated sphere grid and are configured with 45 levels in the vertical and five thickness ice categories, respectively. The atmosphere and land hydrology components are set up on a 50-km polar stereographic mesh with the vertical
145 resolution of 40 levels and 3 soil layers, respectively. For the hindcast simulation (September 1979–present), CFS Reanalysis (CFSR)/CFSv2 are dynamically downscaled to provide RASM-WRF with atmospheric lateral boundary conditions and for linearly increasing grid nudging of winds and temperature for the top half of the model domain, approximately above 540 hPa. The RASM-POP ocean temperature and salinity along the closed lateral boundaries are restored to monthly Polar Science
150 Center Hydrographic Climatology version 3.0 (PHC 3.0; Steele et al., 2001). The initial conditions at the beginning of the hindcast simulation are derived from the 32-year spin-up of the ocean-sea ice model forced with the Common Ocean-Ice Reference Experiment Inter-Annual Forcing version 2 (CORE2-IAF; Large and Yeager, 2009) atmospheric reanalysis for 1948-1979.



155 The RASM-DPLE simulations are derived by dynamically downscaling global atmospheric output from
the initialized CESM-DPLE simulations (Yeager et al., 2018). Output from the two 10-member decadal
ensembles, initialized on December 1st of 1985 and 2015, was selected for in-depth analysis under
different regimes of the Arctic SIT distribution. Each RASM-DPLE simulation is initialized with the
ocean and sea ice conditions, with thinner ice in the latter period (Fig. S1), from the RASM hindcast
160 and integrated for 121 months with CESM-DPLE atmospheric forcing. The size of each ensemble (10
members) is determined by the availability of archived CESM-DPLE output necessary for RASM-WRF
boundary conditions. Hence, output for 100 winters per each ensemble allows for statistical analysis of
polynya occurrence in the past and near future.

3.2 Self-organizing maps

165 The self-organizing map (SOM), an artificial neural network based on a competitive learning algorithm
(Kohonen, 2001), has been widely used to visualize input data vectors onto a low dimensional map of
nodes and to objectively classify complex data sets in meteorology and oceanography (see Liu and
Weisberg, 2011). For January-March 2018, the RASM/WRF pan-Arctic (>65 °N) 6-hourly surface
wind fields (i.e., 10 m U and V components) are characterized using a SOM [4×4] map grid (i.e., 16
170 nodes or patterns). Time-dependent spatial features of near surface winds are identified and frequencies
of occurrence of wind patterns favorable for a polynya are quantified using the SOM Toolbox 2.0 for
MATLAB available at <http://www.cis.hut.fi/projects/somtoolbox>.

4 Results

4.1 2018 winter polynya – a case study

175 4.1.1 Near-surface air temperature around Greenland

Focusing on the most recent and the largest winter polynya event, daily near-surface air temperatures
were examined from the weather stations around the Greenland coast for January-March 2018 (Fig. 3).
A significant warming event (air temperatures rising above 0 °C) was observed over the northeastern
Greenland region from mid-February to early March and captured well in the RASM simulation. This
180 anomalous warming was most prominent along the northern Greenland coast (Figs. 3e and 3f), where
the polynya was observed and simulated in RASM (Figs. 2a and 2d, respectively), but less pronounced
over the mid-eastern Greenland coast (Figs. 3g and 3h). In contrast, no warming was measured in the
southwestern stations for the same period (Figs. 3b-3d). This anomalous warming, with relative
humidity rising above 90% (i.e., Station 04312; not shown), coincided with a strong reversal of the
185 Arctic Oscillation (AO) index from a positive to a strongly negative phase (Fig. 3a). Among the
northeastern stations, the observed near-surface air temperature was positively correlated to the AO
index (Fig. 3i). The maximum correlation coefficient (r) was time-lagged up to 11 days at the northern
stations and only 3-4 days at the mid-eastern stations (Fig. 3j). Given that the anomalous warming
started a few days earlier at the mid-eastern stations and ceased a few days later at the northern stations,



190 it may suggest the advection of warm air masses from the south. The prolonged warming at the northern
stations could also be partly due to the release of oceanic heat from the polynya to the atmosphere.

On the other hand, near-surface air temperatures were inversely correlated with the AO index (Fig. 3i)
in the southwestern Greenland region, with a shorter time-lag (one to two days) for a maximum
195 correlation coefficient (Fig. 3j). We found that no anomalous warming was present in the southwestern
Greenland region during February. In fact, near-surface air temperatures tended to gradually decrease
from January through February, with the lowest temperatures observed between 22nd and 24th of
February 2018 (Figs. 3b-3d). Thereafter, near-surface air temperatures rapidly increased at all
southwestern stations, peaking in early March, corresponding to the strong negative AO phase, and the
200 second warming came approximately two to three weeks later.

Overall, the RASM hindcast simulation captured remarkably well the sudden increase of near-surface
air temperatures in northeastern Greenland and its gradual decrease. RASM also reproduced well the
cooling in February and then the warming over southwestern Greenland, in terms of its magnitude,
205 timing, and spatio-temporal variability (Fig. 3). One discrepancy in the RASM simulation against the
weather stations data was a positive bias of near-surface air temperatures at Stations 04221 (Fig. 3b) and
04330 (Fig. 3g), possibly linked to the relatively coarse horizontal resolution of the RASM atmospheric
component (i.e., 50 km), which is insufficient for resolving strong temperature gradients across the
ocean/land/ice sheet boundary or the fidelity of the near surface temperature distribution over the
210 Greenland Ice Sheet.

4.1.2 Sea ice dynamics

The sudden anomalous warming over northern Greenland with temperatures above 0 °C was an extreme
phenomenon in 2018, considering that the long-term mean (2011-2020) of February surface air
temperature is -27.8 °C at Station 04301 (Fig. 3e; Cape Morris Jesup). In addition, there were other
215 years of anomalous warming (Figs. 4b and 4c), albeit less pronounced, when previous, smaller, polynya
events occurred during February 2011 and 2017 (Figs. 2b and 2c, respectively). The RASM's realistic
representation of the polynya, although the center of the simulated polynya is not exactly located as the
observed one, as well as the magnitude and timing of anomalous warming, grants confidence to the
examination of relative contribution of thermodynamic ice melt to the generation of the polynya. Figure
220 5 shows the RASM thermal sea ice surface, lateral and bottom melting terms were all negligible (< 1
cm) over the study region when integrated for the whole month of February 2018. Hence, the dramatic
rise of near-surface air temperatures by more than 25 °C above climatology and their persistence around
the freezing point for several days (Fig. 3e), had no impact on sea ice melt, nor on the preconditioning
and development of the polynya north of Greenland. In agreement with Moore et al. (2018), we
225 corroborate that this polynya was driven by mechanical redistribution of sea ice outside of the study
region (see Fig. 4a): i.e., this was a latent heat polynya. Based on RASM results, we calculate that
between 15 and 25 February 2018, 192 km³ of sea ice was dynamically transported outside the study
region (Fig. 4d). During two weeks prior to the 2018 polynya event, a mean thermodynamic ice growth
over the region was 0.72 km³/day (Fig. 4d), which is comparable to the rate in a non-polynya year such



230 as 2019 (not shown). The peak sea ice growth of $3.1 \text{ km}^3/\text{day}$ occurred on 26 February right after the
maximum daily dynamic ice removal and the anomalous warming period. However, this large sea ice
removal due to the polynya was not fully replenished in the region by the end of March, even with
dynamic and thermodynamic processes adding 81 km^3 and 42 km^3 , respectively, after 26 February.
Overall, the RASM integrated thermodynamic ice growth in the study region during February 2018 was
235 approximately 50% higher (31.2 km^3 ; Fig. 4d) due to the rapid ice growth during the polynya opening,
compared to the ice growth during a non-polynya year (i.e., 20.8 km^3 in February 2019; not shown).

4.1.3 Atmospheric-sea ice coupling

As dynamic processes dominated the overall winter sea ice in the study region, we have analyzed the
wind data from the weather station (Station 04301; Station Nord) and have found that the polynya
240 development was associated with strong and persistent winds from the south-southeast (Fig. 4g). We
further examined how the spatial near-surface wind fields evolved over the time period associated with
the sea ice divergence. The SOM analysis extracted 16 patterns from the total of 360 synoptic wind
fields: the 6-hourly RASM 10 m U- and V-wind components during January-March 2018. Figure 6
shows the four major wind patterns most frequently identified (more than 77% occurrence) from the
245 pre-polynya period (5 February 2018) until closing of most of open water areas (13 March 2018). The
RASM hindcast simulation confirmed that this polynya event was predominantly associated with
southerly to southeasterly winds blowing over the northern Greenland region (Fig. 6b and 6c),
consistent with the ERA-Interim reanalysis of 10 m wind fields (Fig. S2). Prior to the polynya event in
2018, surface winds were mainly from the north or northwest over the region (Fig. 6a), which yielded
250 little or no sea ice divergence (Fig. 6e). When the major wind pattern shifted to between southerly to
southeasterly winds over the northern Greenland region on 15 February 2018 (Fig. 6b), sea ice started to
deform and diverge significantly (Fig. 6f). Beginning on 20 February 2018, the southeasterly wind
became even more prominent, with 19% stronger wind speed over the northern coast of Greenland (Fig.
6c), which increased the sea ice deformation rate further and led to the maximum polynya opening (Fig.
255 6g). The largest observed and modeled polynya areas were identified on 25 February 2018 (see Figs. 2a
and 2d, respectively). Thereafter, within a week, the shift of wind patterns in late February (Fig. 6d)
reversed the dynamic sea ice volume (SIV) tendency from net loss to gain (Fig. 4d) and subsequently
reduced the deformation rate back to nearly zero by early March (Fig. 6h)

260 4.2 Winter polynya events before 2018

Upon examining satellite-derived SIC over the entire data record between 1979 and 2020 (Figs. 7, S3,
and S4), we found that there were two additional polynya events, albeit smaller, over the northern
Greenland region observed in February 2017 and 2011 (see Figs. 2b and 2c, respectively). Here, we
found that a polynya event occurred when the daily mean satellite-derived SIC fell down to or below
265 90%, which occurred for three consecutive days in 2011, one day in 2017, and 10 days in 2018 (see
Figs. 7a, 7g, and 7h, respectively). As was the case of the 2018 polynya, both the previous events also
coincided with anomalous warming, peaking on 12 February 2011 (Fig. 4b) and on 8 February 2017



(Fig. 4c), as measured at Station 04301 (Cape Morris Jesup). Near-surface air temperature variability was statistically correlated with the AO index ($r=0.39$, $p<0.01$ in 2011; $r=0.45$, $p<0.01$ in 2017), lagged by approximately two weeks. Those two polynyas were represented well in the RASM hindcast simulation (Figs. 2e and 2f) and thus we investigated their causality with respect to their relative SIV reductions due to dynamical processes and/or thermodynamic ice melt (Figs. 4e and 4f). The RASM results confirmed that those were latent heat polynyas dominated by the mechanical redistribution of sea ice out of the region. Their sizes were smaller compared to the 2018 polynya, with the one in 2017 even smaller than the one in 2011, which we attribute to somewhat different wind patterns such as its direction, magnitude and duration (Figs. 4i and 4h). Table 1 shows that, during the polynya periods (defined here when ice volume tendency is negative), i.e., 12-15 February 2011 and 8-10 February 2017, 55 km³ and 42 km³ of sea ice was dynamically removed outside the study region, respectively, which is much less compared to the ice loss of 189 km³ during the 2018 event (16-25 February 2018). The size of a polynya was proportional to the pseudo-wind stress (i.e., wind speed squared) integrated over the polynya period (Table 1). Thus, more turbulent (latent plus sensible) heat was lost during the 2011 winter polynya (daily mean of -96.7 W/m² and maximum of -125 W/m²) when its size was bigger (Table 2). In addition, referenced to the February ice growth during a non-polynya year (for example, 20.8 km³ in February 2019; not shown), the RASM thermodynamic ice growth integrated over the month of February was elevated: 33% higher in 2011 (27.6 km³; Fig. 4f) in the study region. Note that the daily mean turbulent heat flux in the study region was -48 W/m² during the 2018 winter polynya event with the maximum daily heat loss up to -182 W/m². However, the total daily turbulent heat loss was much larger than any other year because of the size and duration of open water areas (Table 2).

Given the above analysis, an outstanding question is why winter polynyas was only observed during the 2010s within the past four decades. Since observational data around northern Greenland are incomplete for the whole period of 1980-2020, we expanded the analysis of surface wind fields (10 m U and V components) from the RASM hindcast simulation near Station 04312 (Fig. 8a; Station Nord) and Station 04301 (Fig. 8b; Cape Morris Jesup). Our analysis revealed that northward wind (blowing from south), required for opening of a winter polynya along the coast of northern Greenland, has recently become more frequent, stronger (i.e., wind speed >10 m/s), and more persistent (i.e., blowing for at least 2 consecutive days or longer). In addition, the three years of winter polynya occurrence with the wind conditions satisfying the above criteria, all coincidentally were La Niña winters (see https://origin.cpc.ncep.noaa.gov/products/analysis_monitoring/ensostuff/ONI_v5.php). Based on the RASM hindcast simulation, the grid mean wind conditions in February 2009 were similar to the ones in February 2017 near Station 04312 (Fig. 8a), but a notable polynya was not detected, possibly owing to the influence by such wind conditions over a smaller area within the main polynya region. The observational data also indicate a polynya favorable wind condition in 2009: i.e., relatively warmer air (-12.6 °C) blowing from the south-southwest with the maximum wind speed of 19 m/s on February 7th, 2009 at Station 04312 (Table S1). But, the satellite-derived mean daily SIC only dropped down to 94% in February 2009 (Fig. S4o) because the wind was possibly weaker, compared to the wind condition in February 2017 (Fig. 4i). Note that the early February 2009 data at Station 04312 are missing and the entire February 2009 data at Station 04301 are completely unavailable.



310

4.3 Polynyas in a large ensemble of initialized decadal prediction simulations

According to the merged CryoSat-2/SMOS data, the mean SIT over the region does not exhibit a negative trend in February. For example, in the first week of February, the mean SIT was 2.74 m in 2011, 3.16 m in 2017, and 2.73 m in 2018. On the other hand, the RASM hindcast simulation indicates a gradual thinning of sea ice in the region and a long-term trend of SIT was -0.26 m/decade for all months during 1985-2019 (not shown). In order to further investigate the potential role of regional sea ice thickness reduction versus internal variability in the occurrence of winter polynya events over north of Greenland, we performed and examined two RASM 10-member ensembles forced with atmospheric output from the CESM-DPLE simulations. They are initialized 30 years apart, i.e. in December 1985 and 2015, respectively, to represent different SIT conditions over the study region, with the former corresponding to a thicker ice regime (Fig. S1a; mean SIT of 3.3 m) and the latter to a thinner ice regime (Fig. S1b; mean SIT of 2.3 m). Note that the PIOMASS SIT also corroborates that sea ice was 1.1 m thicker north of Greenland in November 1985 (Fig. S1d; mean SIT of 3.3 m) than in November 2015 (Fig. S1e; mean SIT of 2.2 m). Each ensemble member is integrated forward for 10 years, thus resulting in 100 winters (i.e., 10 ensemble members for each 10-year simulation) for statistical analysis of polynya occurrence in each of the two ensembles. Note that because of the setup of these experiments (i.e. using the CESM DPLE atmospheric output as boundary conditions for forcing the RASM-DPLE simulations), we only compared the probability of polynya occurrence during winter months (January-March) instead of focusing on accurate temporal representation of such events in a similar location.

Taking as the baseline the winter polynya in February 2017 (Fig. 4e and Table 1), which was the smallest among the three observed events, we defined “a latent heat polynya” in the RASM-DPLE ensemble members when a daily winter sea ice loss due to dynamic processes was greater than 10 km³/day for at least three consecutive days over the study area (see Fig. 4a). Note that the two other observed polynya events experienced 4 and 10 consecutive days of dynamic sea ice loss greater than 10 km³/day during February of 2011 (Fig. 4f) and 2018 (Fig. 4d), respectively (Table 1). Analogous to the RASM hindcast simulation, Table 3 and 4 list all the polynya occurrences from the two ensemble runs. We found 17 polynyas in the 1985-initialized ensemble (Table 3) and 14 polynyas in the 2015-initialized ensemble (Table 4), out of the 100 winters each. Note that some ensemble members simulate more than 1 polynya event while some had no polynya at all. The majority of the polynya events (88% in the 1985-initialized and 64% in the 2015-initialized runs) were similar in size to the smaller polynyas that were simulated in February of 2011 and 2017. The longer-lasting polynyas (with dynamic sea ice removal of 10 km³/day or greater for five consecutive days or longer) were also produced in the RASM-DPLE simulations: two incidents in the 1985-initialized and four incidents in the 2015-initialized runs. But none of the ensemble members produced the total integrated turbulent heat flux as large as the 2018 polynya (Table 2).

We finish this analysis of RASM-DPLE results by comparing the largest polynya detected in each ensemble (see Table 3 and 4), i.e., from the ensemble member #4 in January 1988 (Fig. 9a) and the



ensemble member #2 in January 2024 (Fig. 9b). As in the case of observed events, these latent heat polynyas were created due to dynamic sea ice transport ($DVT \leq -10 \text{ km}^3/\text{day}$ for seven consecutive days), resulting in significant sea ice removal of -120 km^3 out of the region in 1988 (Fig. 9c; Table 3) and -136 km^3 in 2024 (Fig. 9d; Table 4). By cross-examining wind patterns over northern Greenland (i.e., near Cape Morris Jesup), our analysis confirmed that these large polynya openings were also associated with very strong and persistent southerly winds in the RASM-DPLE simulations (Figs. 9e and 9f). We found that daily DVT and meridional wind were significantly correlated, and the size of polynyas was highly dependent on the pseudo-wind stress integrated over the polynya period (Table 3 and 4). However, given the wind patterns, their duration and the integrated sea ice removal (-189 km^3) during the observed polynya in February 2018 (Table 1), this event stands out within all the RASM results analyzed in this study. Compared to the 2018 event, the slight difference in the magnitudes between the largest polynyas of each ensemble still does not imply much significance of SIT in their generation and evolution. Overall, a similar number of winter polynyas, produced between the two 30-year apart ensembles, implies that changes in SIT are not significant contributors (at least up to now) to the generation of such events for this region during wintertime.

5 Discussion

The dynamic downscaling approach using the high-resolution RASM allows resolving the fine-scale processes and provides valuable insight into the mechanism of generation and evolution of winter polynyas off the northern coast of Greenland. We examined the occurrence of such events in RASM against the satellite observations over the past four decades. The results from the RASM hindcast simulation suggest that the size of a winter latent heat polynya in this region is sensitive to the direction, magnitude and duration of near-surface winds. Subject to the limited sample sizes, we find that the generation of a winter polynya in this region requires strong southerly winds (i.e., speeds greater than at least 10 m/s and lasting for more than 2 days largely over the study region based on the RASM hindcast simulation). Table 1 and Figure 8 show that the stronger and more persistent the southerly wind blows, the larger the winter polynya becomes; however, there were no such extreme weather events before 2010. On the other hand, the southerly winds might reduce sea ice export through Fram Strait by a slowdown of sea ice drift (Wang et al., 2021). It can also be speculated that this region might have been affected by increasing extreme winter storm activities in recent years that are associated with anomalous warming events. However, no significant trends were found in January-February during 1979-2015 (Rinke et al., 2017).

Considering the overall vulnerability and fate of some of the thickest sea ice in the Arctic under the recent warming climate, sea ice may become susceptible to modulation by the atmospheric forcing. However, the RASM-DPLE simulations indicate that the frequency, size and duration of winter polynyas is not affected by sea ice thinning, showing no apparent difference in such polynya characteristics between the two ensembles initialized with two different sea ice regimes 30 years apart: 1980s vs 2010s. For example, the range of 5-day mean SIT before the occurrence of each polynya was $2.9\text{-}4.4 \text{ m}$ (with the mean of 3.8 m and standard deviation of 0.40 m) in the 1985-initialized RASM-



395 DPLE ensemble and 1.8-3.3 m (with the mean of 2.8 m and standard deviation of 0.35 m) in the 2015-
initialized RASM-DPLE ensemble (Table 3 and 4, respectively). Hence, regardless of the SIT decline
over the region, this study suggests that the primary necessary condition for a winter polynya
occurrence is strong and persistent southerly winds. With the maximum wind speed exceeding 20 m/s
and duration for 10 days, the 2018 winter polynya remains unique by any of these metrics.

400 During the 2017-2018 winter, the AO shifted from a positive phase to a strong negative phase between
mid-February to early March (Fig. 3a), which was associated with weakening of the polar vortex and
allowed warmer air into the Arctic. Alternatively, Kim et al. (2014) argued that due to sea ice loss
especially in Barents-Kara seas, the weakened stratospheric polar vortex preferentially induced a
negative phase of the AO at the surface, resulting in warm air into the Arctic. This anomalous warming
event occurred coincidentally after the sudden stratospheric warming (SSW) event observed in mid-
February 2018 (Moore et al., 2018; Rao et al. 2018), which developed into a vortex split (Lü et al.,
2020). Subsequently, the winter weather was severe with intense cold air across Europe in March 2018
405 (Overland et al., 2020). Although the exact cause of SSW variability is still under debate, SSWs are
generally known to cause anomalous warming over Greenland and impact surface weather patterns
down to mid-latitudes (Butler et al., 2017). The frequency of their occurrence is enhanced by El Niño
conditions (Polvani et al., 2017 and also true for La Niña winters depending on SSW definitions (Song
and Son, 2018); for example, La Niña was in winter 2017-2018. In the recent winters with SSW (Butler
410 et al., 2017; Rao et al., 2018; Knight et al., 2021), no winter polynya events occurred except in February
2018.

415 The opening of polynyas in the region between the Wandel and Lincoln seas primarily depends on a
large-scale surface pressure pattern change, resulting in strengthening of intense southerly winds that
are short-lived and sporadic. Toward the end of each polynya event, the rate of thermodynamic ice
growth generally increased (Figs. 4d, 4e and 4f). The maximum rate of ice growth happened not when
sea ice removal was largest with strong southerly wind but when air temperature started to significantly
drop (Fig. 4). Upward surface turbulent heat fluxes continued even after DVT became positive (i.e.,
Table 2 and Fig. 4) when wind direction was reversed (i.e., Fig. 6d) until the open water area was
420 completely covered by ice. In general, the rate of new ice formation in winter is expected to be high
during an open water phase, such as leads and polynyas, due to an intense turbulent heat (sensible and
latent) loss to the atmosphere. In some polynya regions, turbulent heat loss is as high as 300 W/m² such
as along the Weddell Sea coast (see Morales Maqueda et al., 2004). However, mean turbulent heat loss
in the study region was about 48 W/m² in 2018, which is much smaller than that in the St. Lawrence
425 Island polynya (412 W/m²; Pease, 1987) and Okhotsk Sea coast (471 W/m²; Alfultis and Martin, 1987),
but comparable to the Northeast Water (NEW) polynya (31 W/m²; Morales Maqueda et al., 2004).
Nevertheless, new sea ice formation was somewhat slowed down in the study region because the air-sea
temperature difference was much smaller than in the other regions listed above due to the anomalously
warm air carried by southerly winds over the northern Greenland.

430 Finally, unlike the events in 2011 and 2017, sea ice in the northern Greenland region was not fully
restored even a month after the peak ice removal on February 25th, 2018 (Fig. 4d). Based on the RASM



435 simulation between February 1st to March 31st, 2018, the study region lost approximately 208 km³ of sea
ice due to mechanical ice removal. Although sea ice was added later by the dynamic replenishment (102
km³) and the thermodynamic ice growth (64 km³), the deficit of SIV was about 42 km³, which is
equivalent to the 36 cm reduction of mean SIT over the study region. The CryoSat-2/SMOS data also
confirmed the similar sea ice loss in the region; at the end of March 2018, the mean sea ice north of
440 Greenland was relatively thinner (2.45 m), compared to the beginning of February (2.73 m). Hence, one
could hypothesize that the 2018 winter polynya event could have contributed to the preconditioning of
the polynya event in the following summer (Schweiger et al., 2021), which was observed at a similar
location. Hence the winter event might have been unprecedented by yet another measure, as polynya
events have never repeated within a year over the study region except 2018.

6 Summary

445 Following the previous study of the 2018 winter polynya by Moore et al. (2018), this study
demonstrates that all three observed winter open water events occurred under a specific wind pattern,
which removes sea ice mechanically out of the region. In February 2011 and 2017, the wind direction
was primarily from the south and southwest (Figs. 4i and 4h). The size of polynya depended on the
strength and persistence of southerly winds, and the polynya closure was a result of the relaxation of
these conditions. The polynya was larger in February 2011 compared to the one in 2017 because wind
450 duration was longer: 4 days of strong southerly wind (> 10 m/s) in 2011 compared to 2 days in 2017
(Fig. 8a). Hence, 31% more sea ice was removed in the former, although wind speed and wind stress
were similar between the two years (Table 1). The observed polynya in February 2018 was the largest
one over the satellite SIC record since 1979. It resulted from much stronger and more persistent
southerly-southeasterly winds (Fig. 4g) off the coast of northern Greenland, the direction which could
455 also be more favorable for polynya opening (Kawaguchi et al., 2010). Although sea ice was
significantly thicker in the 1980s, more polynyas were not prevalent with thinner ice in the winters of
2015-2025 from the two RASM-DPLE ensembles. Given the similar rate of winter polynya occurrence
and their apparent lack of sensitivity to the initial sea ice thickness, we conclude that a dominant cause
of these winter polynyas stems from internal variability of atmospheric forcing rather than from the
460 forced response to warming climate.

Acknowledgement

This work was funded by NSF OPP IAA1603602 (NPS), DOE RGMA DE-SC0014117 (NPS), NSF
OPP-1603544 (CU Boulder), the Canada 150 Chair program (J. S.), and the Ministry of Science and
Higher Education in Poland (R. O.) in the frame of international project agreement 3808/FAO/2017/0.
465 The PNNL is operated for the U.S. DOE by Battelle Memorial Institute under contract DE-AC05-
76RL01830. In addition, computing resources were provided by the U.S. DOD High Performance
Computer Modernization Program (HPCMP).



Competing interestsCode/data availability

470 All RASM simulations are archived in the HPCMP archive system and will be available upon
publication according to the U.S. DOD data policy.

Competing interests

The authors declare no competing interests.

475 Author contributions

Y. L. and W. M. conceived the study and wrote the paper. A. C., S. K., R. O., and M. S. undertook the implementation and development of the RASM simulation. J. C., J. C. K., J. S., and H. W contributed to the interpretation of results. All authors except S. K. and A. C. commented on the manuscript.

480



References

- Alfultis, M. A., & Martin, S. (1987). Satellite passive microwave studies of the Sea of Okhotsk ice cover and its relation to oceanic processes, 1978–1982. *Journal of Geophysical Research: Oceans*, 92(C12), 13013–13028.
- Bintanja, R., & Van der Linden, E. C. (2013). The changing seasonal climate in the Arctic. *Scientific reports*, 3(1), 1–8.
- 485 Butler, A. H., Sjoberg, J. P., Seidel, D. J., & Rosenlof, K. H. (2017). A sudden stratospheric warming compendium. *Earth Syst. Sci. Data*, 9, 63–76. <https://doi.org/10.5194/essd-9-63-2017>
- Cassano, J. J., DuVivier, A., Roberts, A., Hughes, M., Seefeldt, M., Brunke, M., et al. (2017). Development of the Regional Arctic System Model (RASM): near-surface atmospheric climate sensitivity. *Journal of Climate*, 30(15), 5729–5753.
- 490 Cavalieri, D. J., Gloersen, P., & Campbell, W. J. (1984). Determination of sea ice parameters with the Nimbus 7 SMMR. *Journal of Geophysical Research: Atmospheres*, 89(D4), 5355–5369.
- Craig, A. P., Vertenstein, M., & Jacob, R. (2012). A new flexible coupler for earth system modeling developed for CCSM4 and CESM1. *The International Journal of High Performance Computing Applications*, 26(1), 31–42.
- 495 Dee, D. P., Uppala, S. M., Simmons, A. J., Berrisford, P., Poli, P., Kobayashi, S., et al. (2011). The ERA-Interim reanalysis: Configuration and performance of the data assimilation system. *Quarterly Journal of the royal meteorological society*, 137(656), 553–597.
- DuVivier, A. K., Cassano, J. J., Craig, A., Hamman, J., Maslowski, W., Nijssen, B., et al. (2016). Winter atmospheric buoyancy forcing and oceanic response during strong wind events around southeastern Greenland in the Regional Arctic System Model (RASM) for 1990–2010. *Journal of Climate*, 29(3), 975–994.
- 500 Graham, R. M., Cohen, L., Petty, A. A., Boisvert, L. N., Rinke, A., Hudson, S. R., et al. (2017). Increasing frequency and duration of Arctic winter warming events. *Geophysical Research Letters*, 44(13), 6974–6983. <https://doi.org/10.1002/2017GL073395>.
- Grosfeld, K.; Treffeisen, R.; Asseng, J.; Bartsch, A.; Bräuer, B.; Fritsch, B.; Gerdes, R.; Hendricks, S.; Hiller, W.; Heygster, G.; Krumpen, T.; Lemke, P.; Melsheimer, C.; Nicolaus, M.; Ricker, R. and Weigelt, M. (2016), Online sea-ice knowledge and data platform <www.meereisportal.de>, Polarforschung, Bremerhaven, Alfred Wegener Institute for Polar and Marine Research & German Society of Polar Research, 85 (2), 143–155, doi:10.2312/polfor.2016.011.
- 505 Hamman, J., Nijssen, B., Brunke, M., Cassano, J., Craig, A., DuVivier, A., et al. (2016). Land surface climate in the regional Arctic system model. *Journal of Climate*, 29(18), 6543–6562.
- 510 Hamman, J., Nijssen, B., Roberts, A., Craig, A., Maslowski, W., & Osinski, R. (2017). The coastal streamflow flux in the Regional Arctic System Model. *Journal of Geophysical Research: Oceans*, 122(3), 1683–1701.
- Itkin, P., Spreen, G., Cheng, B., Doble, M., Girard-Ardhuin, F., Haapala, J., et al. (2017). Thin ice and storms: Sea ice deformation from buoy arrays deployed during N-ICE2015. *Journal of Geophysical Research: Oceans*, 122(6), 4661–4674.
- 515 Kawaguchi, Y., Nihashi, S., Mitsudera, H., & Ohshima, K. I. (2010). Formation mechanism of huge coastal polynyas and its application to Okhotsk northwestern polynya. *Journal of physical oceanography*, 40(11), 2451–2465.
- Kim, B. M., Son, S. W., Min, S. K., Jeong, J. H., Kim, S. J., Zhang, X., ... & Yoon, J. H. (2014). Weakening of the stratospheric polar vortex by Arctic sea-ice loss. *Nature communications*, 5(1), 1–8.
- 520 Knight, J., Scaife, A., Bett, P. E., Collier, T., Dunstone, N., Gordon, M., ... & Walker, B. (2021). Predictability of European Winters 2017/2018 and 2018/2019: Contrasting influences from the Tropics and stratosphere. *Atmospheric Science Letters*, 22(1), e1009.
- Kohonen, T. (2001). *Self-Organizing Maps*, third ed. Springer-Verlag, New York.
- Kwok, R. (2018). Arctic sea ice thickness, volume, and multiyear ice coverage: losses and coupled variability (1958–2018). *Environmental Research Letters*, 13(10), 105005. <https://doi.org/10.1088/1748-9326/aae3ec>
- 525 Kwok, R., Cunningham, G. F., Wensnahan, M., Rigor, I., Zwally, H. J., & Yi, D. (2009). Thinning and volume loss of the Arctic Ocean sea ice cover: 2003–2008. *Journal of Geophysical Research*, 114(C7), C07005. <https://doi.org/10.1029/2009JC005312>.
- Large, W., & Yeager, S. G. (2009). The global climatology of an interannually varying air–sea flux data set. *Climate dynamics*, 33(2–3), 341–364.



- 530 Liu, Y., & Weisberg, R. H. (2011). A review of Self-Organizing Map applications in meteorology and oceanography. In *Self-Organizing Maps - Applications and Novel Algorithm Design*, Edited by J. I. Mwasiagi, InTech, Rijeka, Croatia, ISBN 978-953-307-546-4, pp.253-272.
- Lü, Z., Li, F., Orsolini, Y. J., Gao, Y., & He, S. (2020). Understanding of European cold extremes, sudden stratospheric warming, and Siberian snow accumulation in the winter of 2017/18. *Journal of Climate*, 33(2), 527-545.
- 535 Ludwig, V., Spreen, G., Haas, C., Istomina, L., Kauker, F., & Murashkin, D. (2019). The 2018 North Greenland polynya observed by a newly introduced merged optical and passive microwave sea-ice concentration dataset. *Cryosphere*, 13(7).
- Maslowski, W., Kinney, J. C., Higgins, M., & Roberts, A. (2012). The future of Arctic sea ice. *Annual Review of Earth and Planetary Sciences*, 40.
- 540 Maykut, G. A. (1982). Large-scale heat exchange and ice production in the central Arctic. *Journal of Geophysical Research*, 87(C10), 7971. <https://doi.org/10.1029/JC087iC10p07971>.
- Meier, W. N., Fetterer, F., Savoie, M., Mallory, S., Duerr, R., & Stroeve, J. (2017a). *NOAA/NSIDC Climate Data Record of Passive Microwave Sea Ice Concentration, Version 3*. Boulder, Colorado USA. NSIDC: National Snow and Ice Data Center. doi: <https://doi.org/10.7265/N59P2ZTG>. Accessed 27 Sep 2019.
- 545 Meier, W. N., Fetterer, F., & Windnagel, A. K. (2017b). *Near-Real-Time NOAA/NSIDC Climate Data Record of Passive Microwave Sea Ice Concentration, Version 1*. doi: <https://doi.org/10.7265/N5FF3QJ6>.
- Meier, W. N., Hovelsrud, G. K., van Oort, B. E. H., Key, J. R., Kovacs, K. M., Michel, C., et al. (2014). Arctic sea ice in transformation: A review of recent observed changes and impacts on biology and human activity. *Reviews of Geophysics*, 52(3), 185–217. <https://doi.org/10.1002/2013RG000431>. Accessed 01 Jul 2020.
- 550 Moore, G. W. K., Schweiger, A., Zhang, J., & Steele, M. (2018). What Caused the Remarkable February 2018 North Greenland Polynya? *Geophysical Research Letters*. <https://doi.org/10.1029/2018GL080902>.
- Morales Maqueda, M. A., Willmott, A. J., & Biggs, N. R. T. (2004). Polynya Dynamics: a Review of Observations and Modeling. *Reviews of Geophysics*, 42(1), RG1004. <https://doi.org/10.1029/2002RG000116>.
- Overland, J., Hall, R., Hanna, E., Karpechko, A., Vihma, T., Wang, M., & Zhang, X. (2020). The polar vortex and extreme weather: the Beast from the East in winter 2018. *Atmosphere*, 11(6), 664.
- 555 Pease, C. H. (1987). The size of wind-driven coastal polynyas. *Journal of Geophysical Research: Oceans*, 92(C7), 7049-7059.
- Peings, Y., Labe, Z. M., & Magnusdottir, G. (2021). Are 100 ensemble members enough to capture the remote atmospheric response to +2° C Arctic sea ice loss? *Journal of Climate*, 34(10), 3751-3769.
- 560 Polvani, L. M., Sun, L., Butler, A. H., Richter, J. H., & Deser, C. (2017). Distinguishing stratospheric sudden warmings from ENSO as key drivers of wintertime climate variability over the North Atlantic and Eurasia. *Journal of Climate*, 30(6), 1959-1969.
- Rampal, P., Weiss, J., Marsan, D., & Bourgoin, M. (2009). Arctic sea ice velocity field: General circulation and turbulent-like fluctuations. *Journal of Geophysical Research*, 114(C10), C10014. <https://doi.org/10.1029/2008JC005227>.
- 565 Rao, J., Ren, R., Chen, H., Yu, Y., & Zhou, Y. (2018). The stratospheric sudden warming event in February 2018 and its prediction by a climate system model. *Journal of Geophysical Research: Atmospheres*, 123(23), 13-332.
- Rinke, A., Maturilli, M., Graham, R. M., Matthes, H., Handorf, D., Cohen, L., et al. (2017). Extreme cyclone events in the Arctic: Wintertime variability and trends. *Environmental Research Letters*, 12(9), 094006.
- 570 Roberts, A., Craig, A., Maslowski, W., Osinski, R., DuVivier, A., Hughes, M., et al. (2015). Simulating transient ice-ocean Ekman transport in the Regional Arctic System Model and Community Earth System Model. *Annals of glaciology*, 56(69), 211-228.
- Saha, S., Moorthi, S., Wu, X., Wang, J., Nadiga, S., Tripp, P., et al. (2011). NCEP Climate Forecast System Version 2 (CFSv2) 6-hourly Products. Research Data Archive at the National Center for Atmospheric Research, Computational and Information Systems Laboratory. <https://doi.org/10.5065/D61C1TXF>.
- 575 Schweiger, A. J., Steele, M., Zhang, J., Moore, G. W. K., & Laidre, K. L. (2021). Accelerated sea ice loss in the Wandel Sea points to a change in the Arctic's Last Ice Area. *Communications Earth & Environment*, 2(1), 1-11.
- Schweiger, A., Lindsay, R., Zhang, J., Steele, M., Stern, H., & Kwok, R. (2011). Uncertainty in modeled Arctic sea ice volume. *Journal of Geophysical Research: Oceans*, 116(C8).
- Serreze, M. C., & Francis, J. A. (2006). The Arctic amplification debate. *Climatic change*, 76(3-4), 241-264.



- 580 Song, K., & Son, S. W. (2018). Revisiting the ENSO–SSW relationship. *Journal of Climate*, 31(6), 2133-2143.
- Spreen, G., Kwok, R., & Menemenlis, D. (2011). Trends in Arctic sea ice drift and role of wind forcing: 1992-2009. *Geophysical Research Letters*, 38(19). <https://doi.org/10.1029/2011GL048970>.
- Steele, M., Morley, R., & Ermold, W. (2001). PHC: A global ocean hydrography with a high-quality Arctic Ocean. *Journal of Climate*, 14(9), 2079-2087.
- 585 Stroeve, J., & Notz, D. (2018). Changing state of Arctic sea ice across all seasons. *Environmental Research Letters*, 13(10), 103001.
- Stroeve, J., Barrett, A., Serreze, M., & Schweiger, A. (2014). Using records from submarine, aircraft and satellites to evaluate climate model simulations of Arctic sea ice thickness. *The Cryosphere*, 8(5), 1839-1854.
- 590 Wang, Q., Ricker, R., & Mu, L. (2021). Arctic sea ice decline preconditions events of anomalously low sea ice volume export through Fram Strait in the early 21st century. *Journal of Geophysical Research: Oceans*, 126(2), e2020JC016607.
- Weijer, W., Veneziani, M., Stössel, A., Hecht, M. W., Jeffery, N., Jonko, A., et al. (2017). Local Atmospheric Response to an Open-Ocean Polynya in a High-Resolution Climate Model. *Journal of Climate*, 30(5), 1629–1641. <https://doi.org/10.1175/JCLI-D-16-0120.1>.
- 595 Yeager, S.G., Danabasoglu, G., Rosenbloom, N.A., Strand, W., Bates, S.C., Meehl, G.A., Karspeck, A.R., Lindsay, K., Long, M.C., Teng, H. and Lovenduski, N.S., 2018. Predicting near-term changes in the Earth System: A large ensemble of initialized decadal prediction simulations using the Community Earth System Model. *Bulletin of the American Meteorological Society*, 99(9), pp.1867-1886.
- 600 Zhang, J., & Rothrock, D. A. (2003). Modeling global sea ice with a thickness and enthalpy distribution model in generalized curvilinear coordinates. *Monthly Weather Review*, 131(5), 845-861.



605

610 Table 1. Characteristics of the polynya events, when daily dynamic sea ice removal is greater than 10 km³/day (i.e., dynamic volume tendency (DVT) ≤ -10 km³/day) for more than three consecutive days, and the corresponding wind condition as well as sea ice thickness (SIT) over northern Greenland from the RASM hindcast simulation (1980-2020).

Year	Date when DVT ≤ -10 km ³ /day (No. of polynya days)	Five-day mean SIT (m) before polynya	Daily Mean DVT (km ³ /day)	Total sea ice removal (km ³)	North-South wind during polynya			Nearest weather station
					Time-integrated Pseudo-wind stress* (m ² /s ² ·day)	Mean speed (m/s)	Max. speed (m/s)	
2011	12-15 Feb (4 days)	3.6	-13.8	-55	476	10.2	15.1	Station Nord
2017	8-10 Feb (3 days)	3.3	-14.0	-42	354	9.5	15.3	Station Nord
2018	16-25 Feb (10 days)	3.2	-18.9	-189	1272	11.1	21.8	Cape Morris Jessup

*only for the northward wind component



615

Table 2. Daily mean net turbulent (sensible and latent) heat flux (W/m^2) and its standard deviation (s.d.) during the polynya events over open water areas (km^2), where sea ice thickness (SIT) is less than 10 cm, from the RASM hindcast and DPLE simulations. The negative values indicate heat loss from the polynya to the atmosphere.

620

RASM Cases	Year	Date	Daily Turbulent Flux (W/m^2)			Daily Open Water Area (km^2)			Total integrated turbulent heat (W)	
			max	mean	s.d.	max	mean	s.d.		
Hindcast	2011	15-18 Feb	-125	-96.7	23.2	601	322	236	-1.25×10^{11}	
	2017	10 Feb	-1.80	-1.59	0.289	172	172	n/a	-2.74×10^8	
	2018	20 Feb-1 Mar	-182	-48.2	49.2	13,000	4,210	4,390	-2.03×10^{12}	
DPLE	1985-initialized ensemble #4	1988	17-21 Jan	-196	-100	67.3	429	309	130	-1.54×10^{11}
	2015-initialized ensemble #2	2024	20-24 Jan	-202	-62.6	43.4	6,090	2,540	2,340	-8.87×10^{11}



625 Table 3. The polynya events, defined when daily dynamic sea ice removal is greater than 10 km³/day
 (i.e., dynamic volume tendency (DVT) ≤ -10 km³/day) for more than three consecutive days, and the
 corresponding wind condition near Cape Morris Jessup as well as sea ice thickness (SIT) over northern
 Greenland from the RASM-DPLE simulation, initialized on December 1st, 1985. A correlation
 coefficient (r) is calculated between daily DVT and North-South wind for January-March and the bold
 630 indicates the largest polynya event.

DPLE ensemble member	Year	Month	No. of days when DVT ≤ -10 km ³ /day	Five-day mean SIT (m) before polynya	Daily mean DVT (km ³ /day)	Total Ice removal (km ³)	North-South wind during polynya			r ($p < 0.01$) between daily DVT and North-South wind (Jan-Mar)
							Time-integrated pseudo-wind stress* (m ² /s ² ·day)	Mean speed (m)	Max. speed (m)	
1	1986	Jan	3	4.1	-16.1	-48	307	9.7	13.6	-0.75
1	1986	Mar	4	4.4	-12.6	-50	31	2.5	4.3	-0.75
1	1988	Mar	3	4.0	-11.5	-35	168	7.4	9.9	-0.75
1	1990	Mar	4	3.5	-15.6	-62	395	8.6	15.5	-0.74
3	1987	Jan	4	3.8	-21.4	-85	475	10.1	19.0	-0.71
4	1988	Jan	7	4.2	-17.2	-120	438	7.6	12.0	-0.65
4	1989	Feb	5	4.0	-20.7	-104	651	11.2	15.7	-0.74
4	1991	Feb	3	3.2	-25.2	-76	550	12.6	17.8	-0.80
5	1986	Jan	4	3.8	-17.0	-68	260	7.3	13.7	-0.68
5	1987	Jan	4	3.5	-16.5	-66	121	4.9	8.5	-0.67
5	1988	Mar	3	3.8	-20.0	-60	121	4.8	11.2	-0.50
6	1994	Feb	4	2.9	-22.0	-88	700	13.0	16.7	-0.74
7	1994	Jan	3	3.8	-14.7	-44	255	8.5	12.3	-0.61
8	1992	Jan	3	4.3	-13.6	-41	277	9.2	15.0	-0.73
8	1995	Jan	3	3.3	-16.9	-51	172	6.9	13.0	-0.66
9	1995	Mar	3	3.8	-16.3	-49	322	10.2	11.6	-0.62
10	1987	Feb	3	3.6	-13.2	-40	145	6.6	10.1	-0.59

* only for the northward wind component

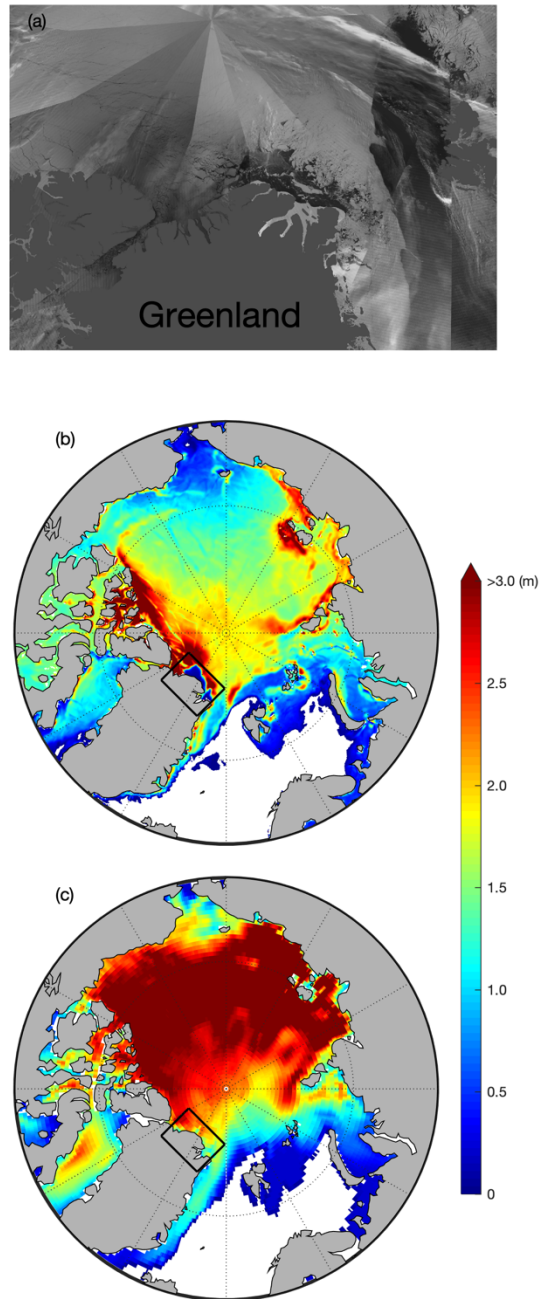


635

Table 4. Same as Table 3, but for the RASM–DPLE simulation, initialized on December 1st, 2015.

DPLE ensemble member	Year	Month	No. of days when DVT ≤ -10 km ³ /day	Five-day mean SIT (m) before polynya	Daily mean DVT (km ³ /day)	Total Ice removal (km ³)	North-South wind during polynya			r ($p < 0.01$) between daily DVT and North-South wind (Jan-Mar)
							Time-integrated pseudo-wind stress* (m ² /s ² ·day)	Mean speed (m)	Max. speed (m)	
1	2016	Feb	5	2.7	-14.4	-72	165	5.0	10.1	-0.75
1	2022	Feb	3	2.6	-15.1	-45	216	8.2	11.5	-0.63
1	2023	Jan	3	2.5	-14.4	-43	321	10.0	14.3	-0.82
1	2023	Jan	3	1.8	-15.4	-46	299	9.8	13.1	-0.82
2	2016	Jan	3	2.8	-16.4	-49	192	7.8	10.9	-0.77
2	2024	Jan	7	3.3	-19.4	-136	841	9.8	19.2	-0.79
4	2019	Mar	3	3.0	-15.4	-46	235	7.4	16.9	-0.65
5	2018	Jan	5	3.0	-20.8	-104	740	10.8	17.9	-0.8
5	2018	Mar	3	3.0	-15.4	-46	129	5.6	12.9	-0.8
5	2020	Feb	5	3.0	-15.5	-77	379	8.4	12.2	-0.75
6	2016	Jan	4	2.8	-12.1	-48	379	9.6	12.3	-0.78
6	2024	Jan	4	2.8	-20.0	-80	352	8.1	15.2	-0.72
8	2017	Feb	3	2.9	-14.5	-43	558	13.1	17.0	-0.8
8	2025	Jan	5	2.8	-18.5	-92	531	9.9	15.8	-0.74

* only for the northward wind component



640

Figure 1: (a) The Visible Infrared Imaging Radiometer Suite (VIIRS) Nighttime Imagery (Day/Night Band, Enhanced Near Constant Contrast) over the northern Greenland on 24 February 2018 (adapted from NASA Worldview at <https://worldview.earthdata.nasa.gov>) and sea ice thickness from (b) the RASM hindcast simulation as well as (c) CFS version 2 reanalysis over the Arctic on 25 February 2018. The rectangular box indicates the polynya area.

645

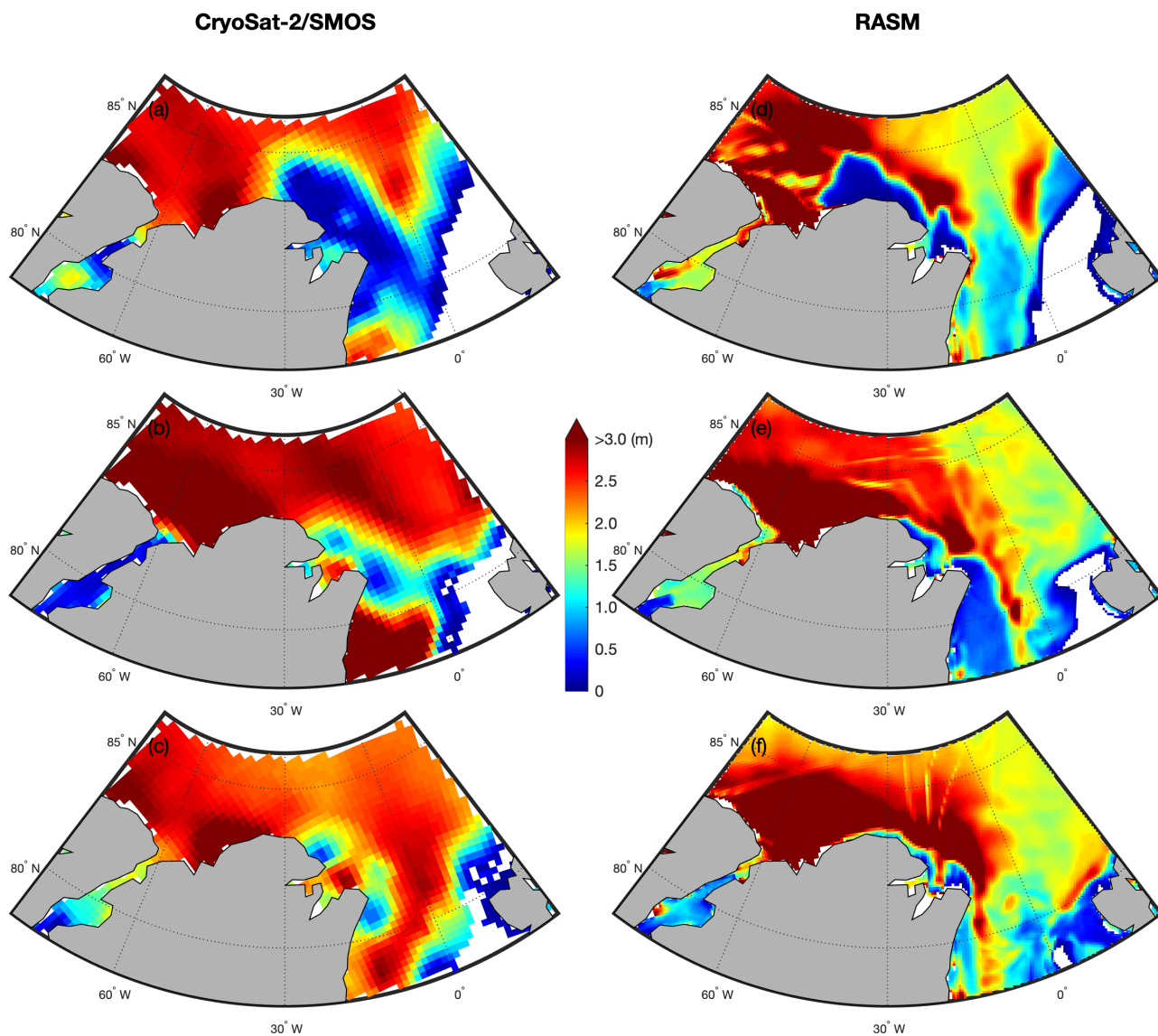
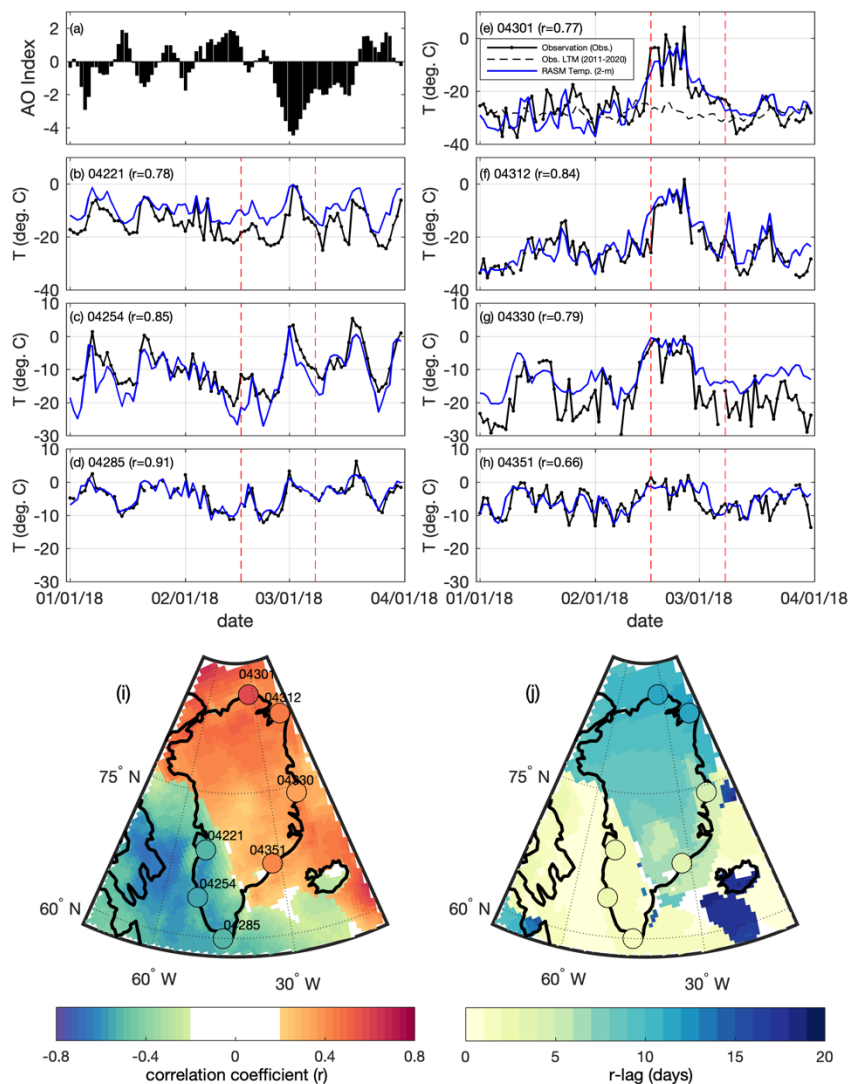


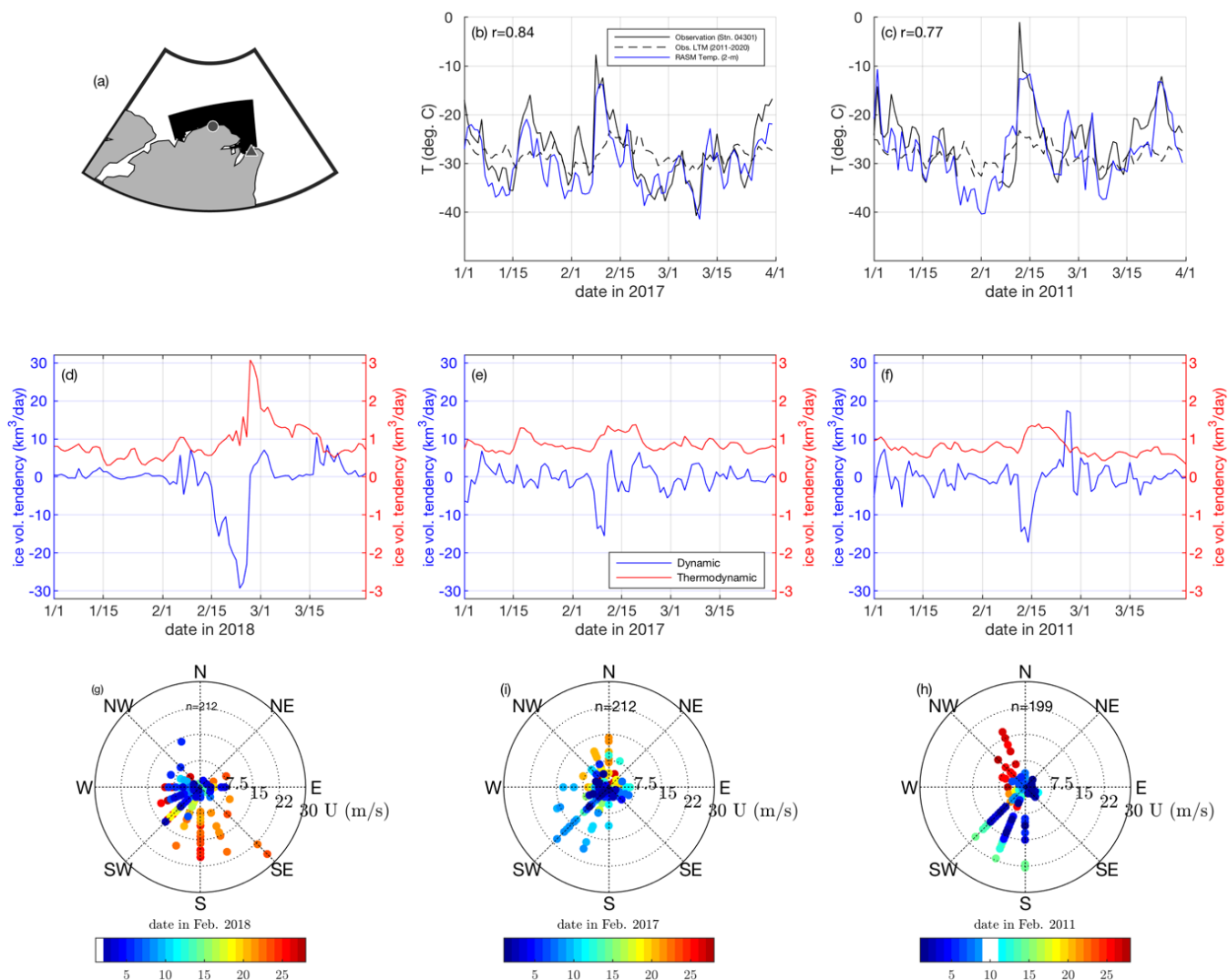
Figure 2: Mean sea ice thickness (SIT) over the northern Greenland region from the CryoSat-2/SMOS merged product on (a) 22-28 February 2018, (b) 8-14 February 2017, and (c) 13-19 February 2011 as well as daily SIT from the RASM hindcast simulation on (d) 25 February 2018, (e) 11 February 2017, and (f) 16 February 2016.



655

660

Figure 3. (a) The observed daily AO index and (b)–(h) the daily mean near-surface air temperature (T , °C; black) during January–March 2018 from the selected weather stations around Greenland as shown in (i) and (j) as circle markers. The RASM daily 2-m air temperature (blue) is from the nearest grid cell and the observed long-term daily mean (LTM, 2011–2020; black-dashed) is only at Station 04301. The correlation coefficient (r) is statistically significant ($p < 0.05$) between the observed and the simulated air temperature is shown in the upper-left. The vertical lines (red-dashed) indicate the start and end dates of the 2018 winter polynya period. The spatial maps show (i) the maximum correlation coefficients and (j) their lagged time-scales (days) between the AO index and the RASM air temperature. Note that grid cells not statically significant ($p > 0.05$) are indicted as white. The color-scale of the markers quantifies the relationship between the AO index and the observed air temperature at each weather station.



665 **Figure 4.** The observed daily near-surface air temperature (T , °C; black) from Station 04301 (Cape Morris Jesup as ●) in (a) and
 the RASM daily 2-m air temperature (blue) from the nearest grid cell during January-March of (b) 2017 and (c) 2011; the
 observed long-term daily mean (LTM, 2011-2020; black-dashed). The correlation coefficient (r) between the observed and the
 simulated air temperature is shown in the upper-left. Time rate of change of the RASM daily sea ice volume (km^3/day) due to
 670 thermodynamic (red) and dynamic (blue) tendency during January-March of (d) 2018, (e) 2017, and (f) 2011, spatially integrated
 for the black-shaded area in (a). Wind rose plots of 3-hourly wind data at Station 04312 (Station Nord as ▲) during February of
 (g) 2018, (h) 2017, and (i) 2011: wind speed (U , m/s) and direction. The missing data are indicted as white in each color bar.

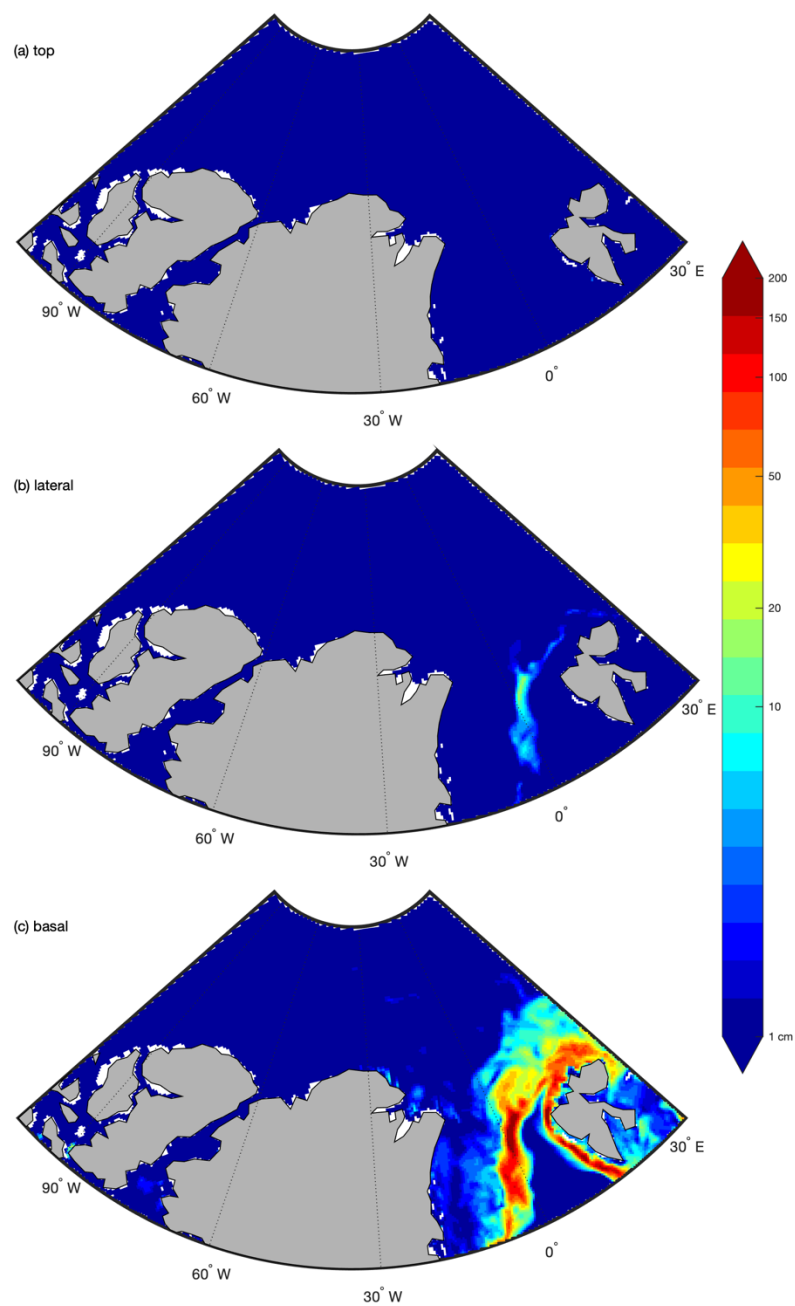
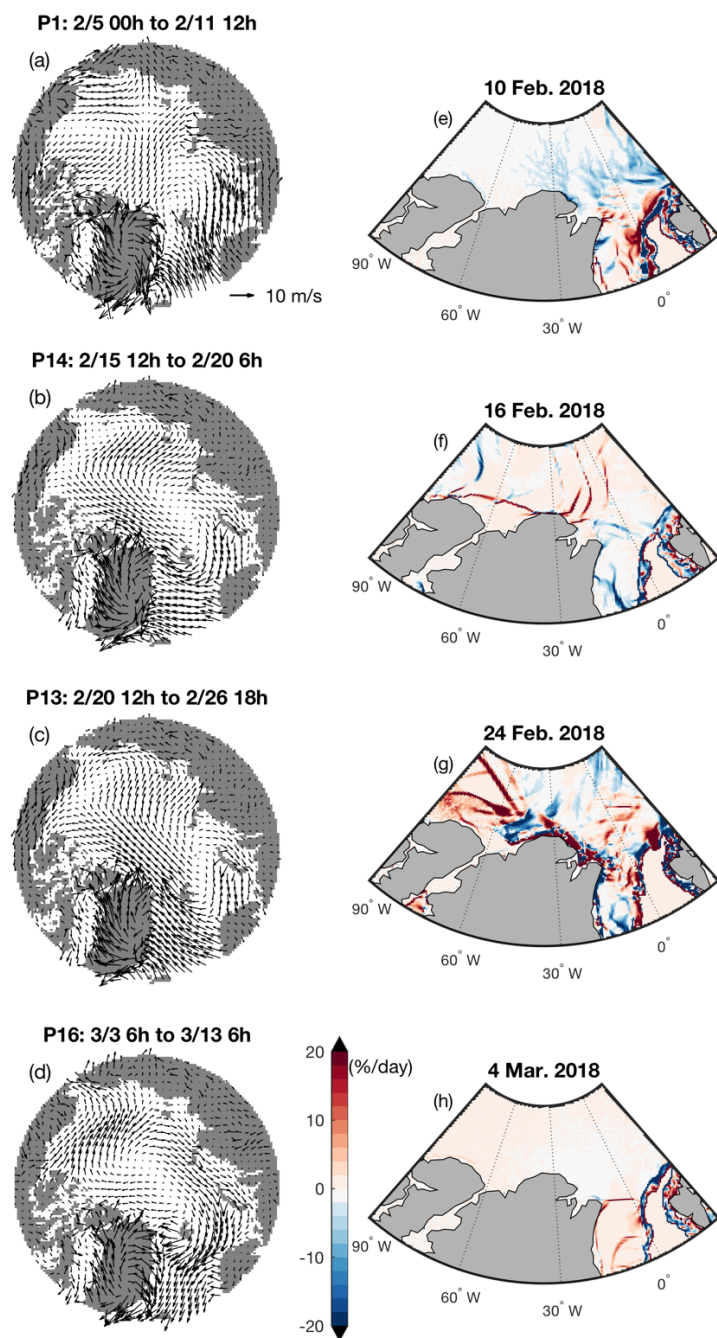


Figure 5. Monthly integrated sea ice melt terms over the northern Greenland region during February 2018 from the RASM hindcast simulation: (a) surface top, (b) lateral, and (c) basal melt (cm).



675



680

Figure 6. Four major patterns with self-organizing maps (frequency of occurrence as %) of the near-surface 6-hourly wind fields from the RASM simulation during the time periods including before and after the 2018 polynya event: (a) 5–11 February (93%), (b) 15–20 February (83%), (c) 20–26 February (93%), and (d) 3–13 March (95%). The wind vectors were sub-sampled at every 3 grid-cells for a plotting purpose. RASM daily sea ice divergence (%/day) within each period above is shown on (e) 10 February, (f) 16 February, (g) 24 February, and (h) 4 March 2018.

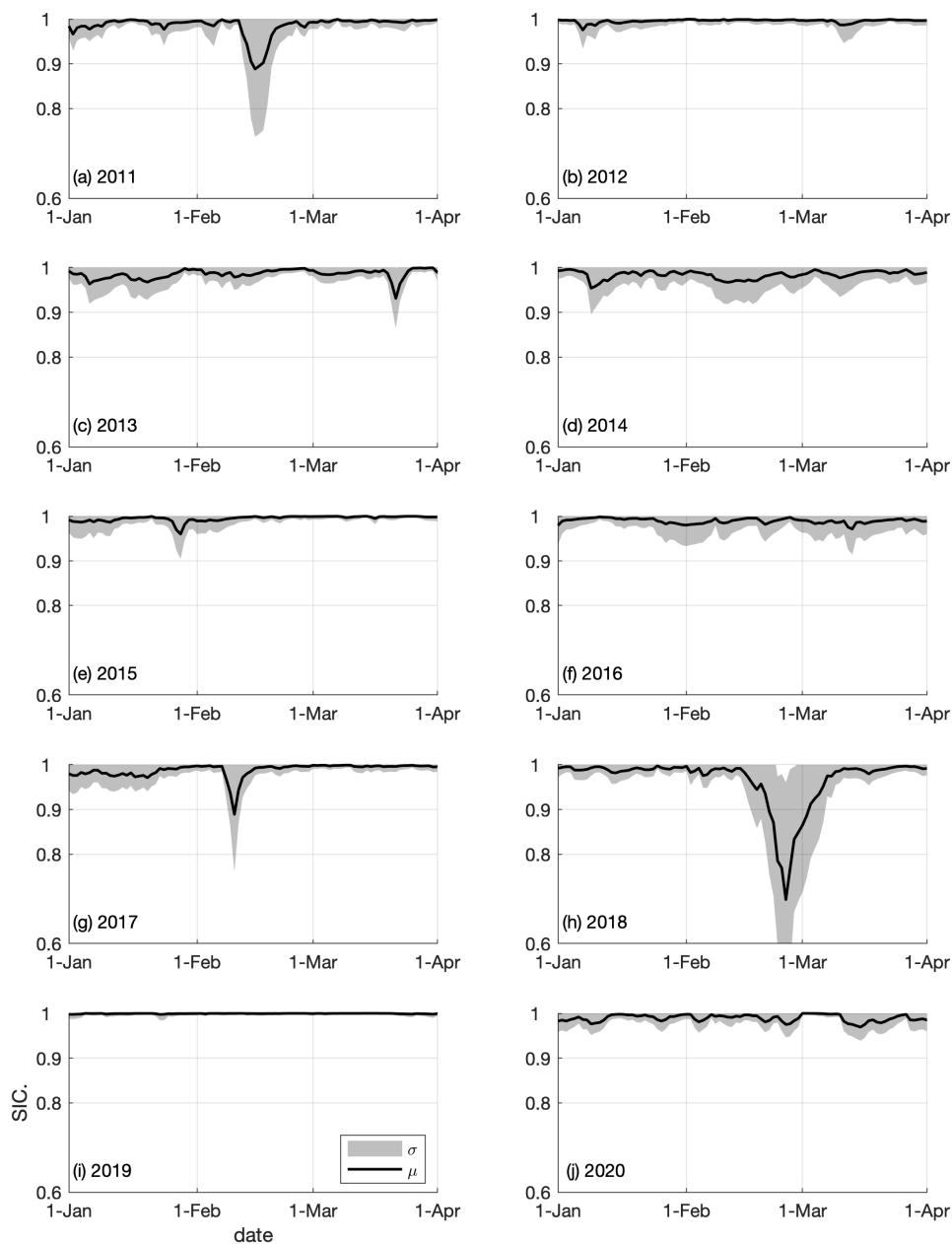


Figure 7. (a)-(j) Satellite-derived (NASA team algorithm) daily mean sea ice concentration (SIC, μ ; black) for the northern Greenland region (see Fig. 4a) during January-March from 2011 to 2020. The grey shading depicts one standard deviation (σ ; gray) from the mean.

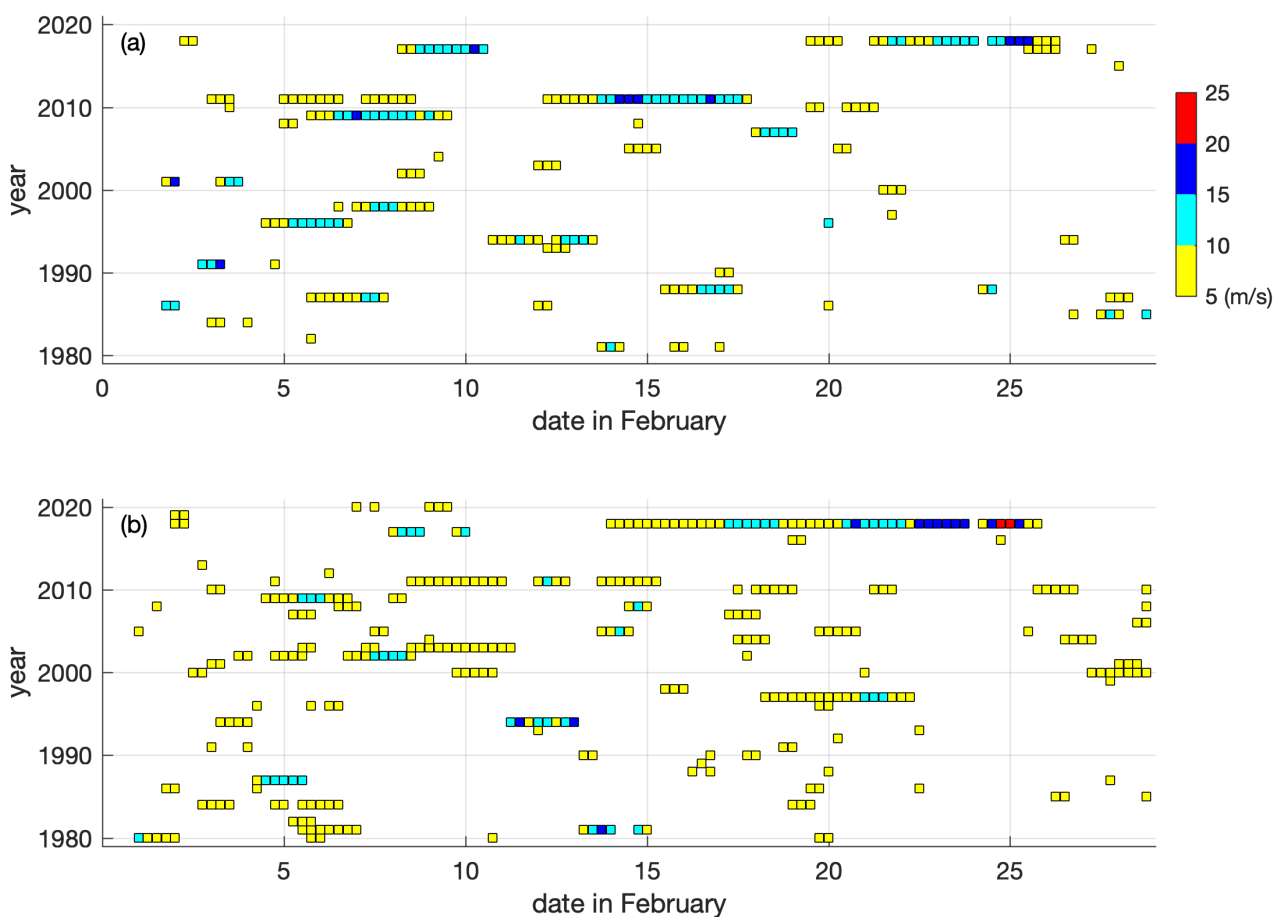


Figure 8. The northward wind component greater than 5 m/s from the RASM hindcast simulation during February of 1980-2020 at the nearest grid to (a) Station 04312 (Station Nord) and (b) Station 04301 (Cape Morris Jesup). Each square represents the six-hourly surface wind and its color indicates a magnitude of wind speed.

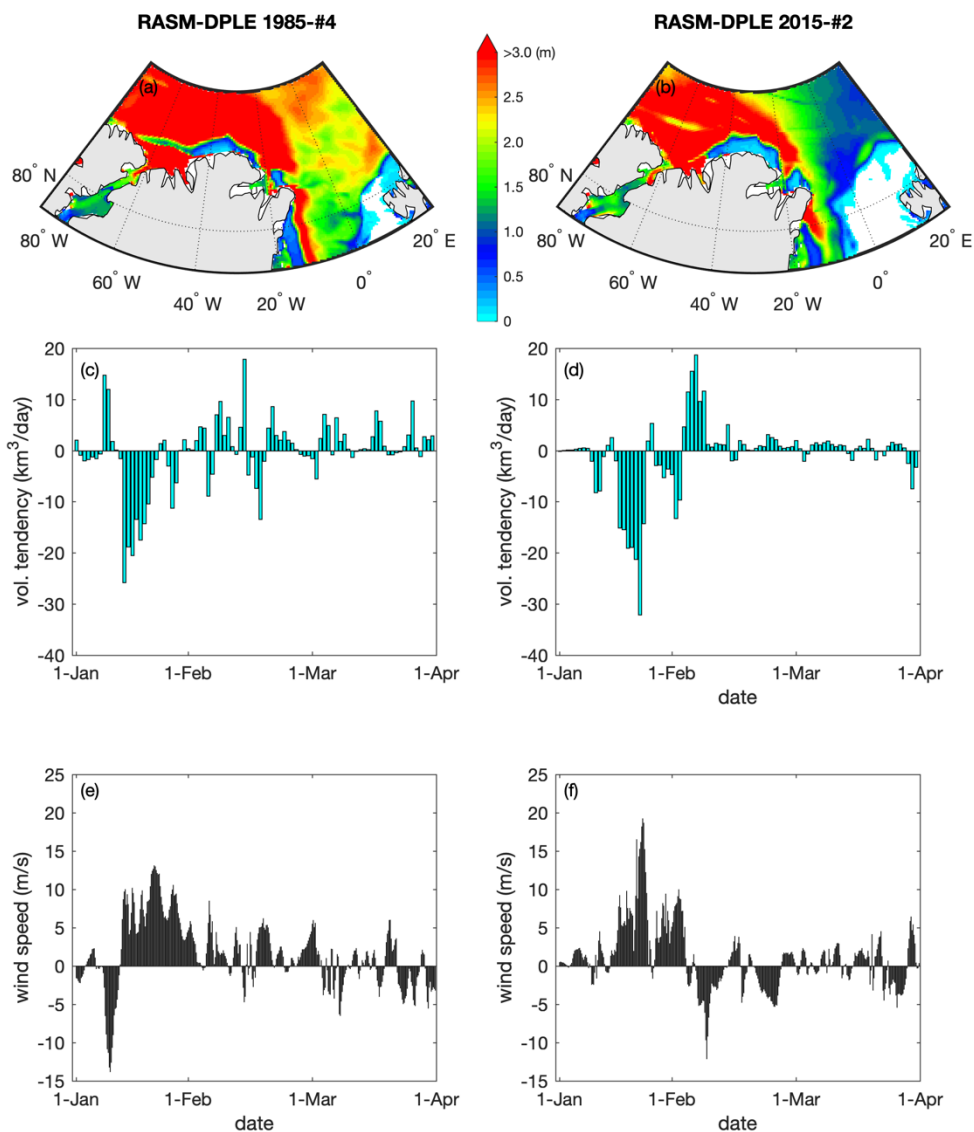


Figure 9. Sea ice thickness (SIT, m), sea ice dynamic volume tendency (DVT, km³/day) for the northern Greenland region (see Fig. 4a), and north(positive)-south(negative) wind component (m/s) during winter months from the ensemble member #4 in the 1985-initialized run and the ensemble member #2 in the 2015-initialized run: SIT on (a) 22 January 1988 and (b) 14 January 2024, daily DVT in January-March of (c) 1988 and (d) 2024, and six-hourly north-south wind in January-March of (e) 1998 and (f) 2024.